Carbon Quantum Dot/TiO<sub>2</sub> Nanohybrids: Efficient
Photocatalysts for Hydrogen Generation via Intimate
Contact and Efficient Charge Separation

Yulu Zhou, \*a Sizhuo Yang, b Donghua Fan, Jake Reilly, Hongwei Zhang, Wei Yao, and Jier Huang \*b

<sup>a</sup>College of Science, China University of Petroleum (East China), Qingdao, 266580, China

<sup>b</sup>Department of Chemistry, Marquette University, Milwaukee, Wisconsin 53201, United States

<sup>c</sup>School of Applied Physics and Materials, Wuyi University, Jiangmen, 529020, China

ABSTRACT. In this work, we report a facile synthesis of carbon quantum dots (CQDs) sensitized TiO<sub>2</sub>/Pt nanocomposites as efficient and robust photocatalysts for light-driven proton reduction from water. We show that this method not only simplifies the synthetic procedure for such hybrid materials but also enhance the direct interaction between CQDs and TiO<sub>2</sub>, which facilitates charge transfer from CQDs to TiO<sub>2</sub> and eventually improves its performance for light-driven H<sub>2</sub> generation reaction. To the best of our knowledge, this work represents the system with highest H<sub>2</sub> generation efficiency among all CQDs sensitized materials.

KEYWORDS: Photocatalytic H<sub>2</sub> generation, carbon quantum dots, heterogeneous nanohybrids, charge separation dynamics, visible light illumination

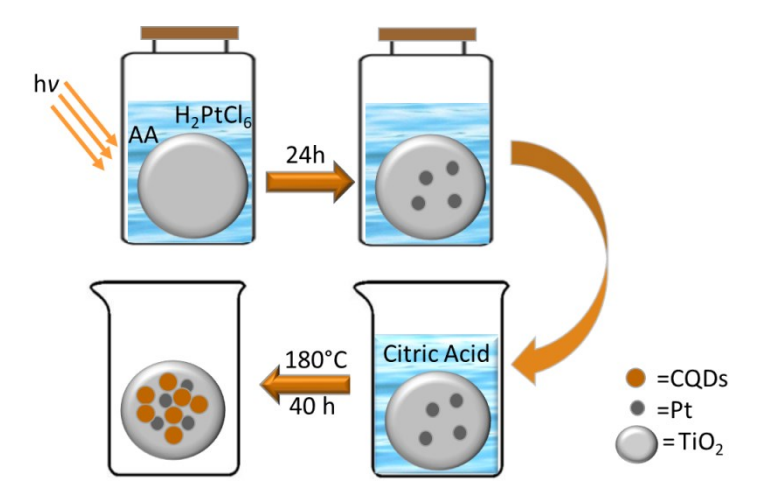
## 1. Introduction

The Photocatalytic generation of H<sub>2</sub> from water through artificial photosynthesis is a viable approach to partially address the energy crisis and environmental issues. 1-2 Since its initial report back to 40 years ago,<sup>3</sup> various photocatalytic systems based on semiconductor materials have been developed. Among them, TiO<sub>2</sub> is the most attractive materials that have been extensively studied because of its low cost, high chemical stability, and nontoxicity. 4-5 However, the largescale application of TiO<sub>2</sub> as photocatalysts for H<sub>2</sub> generation is limited by its wide bandgap (~ 3.2 eV) and poor interfacial charge separation due to rapid electron-hole recombination. Recent efforts have been devoted to address these limitations to optimize its photocatalytic performance.<sup>6-7</sup> For example, enhanced activity has been achieved through band gap sensitization of TiO<sub>2</sub> by molecular dyes<sup>8-9</sup> or introducing impurity atoms into TiO<sub>2</sub>. <sup>10-12</sup> However, these systems either suffer from facile photodegradation or introducing additional defect states which counteract the enhanced visible light absorption. On the other hand, semiconductor nanoparticles such as CdS<sup>13</sup> and PbSe<sup>14</sup> have been introduced as photosensitizers for TiO<sub>2</sub> to extend their light absorption to visible region. However, these materials often contain highly toxic element (Cd or Pd), largely limiting their practical application.

Carbon quantum dots (CQDs) have emerged as a new class of photosensitizers for TiO<sub>2</sub> due to their unique properties including broad full solar spectrum absorption, high stability, and excellent photoinduced charge separation properties etc.<sup>15-17</sup> CQDs embedded/coupled TiO<sub>2</sub> nanostructures (CQDs/TiO<sub>2</sub>) have been used as catalysts for various reactions including dye

degradation, photocatalytic H<sub>2</sub> generation, and liquid phase of alcohols etc. <sup>15, 18-25</sup> While these examples largely demonstrate the promise of CQDs to enhance light absorption property of TiO<sub>2</sub>, CQDs/TiO<sub>2</sub> nanocomposites in these stems were fabricated via multiple-step hydrothermal method, i.e. CQDs/TiO<sub>2</sub> nanocomposites were made directly from pre-synthesized CQD and TiO<sub>2</sub>, which not only involves complex synthetic procedure but also results in the poor contact between CQDs and TiO<sub>2</sub>. <sup>26-28</sup>

To address the issues mentioned above, in this work, we report a novel one-step method for fabrication of CQDs/TiO<sub>2</sub> heterostructure by co-thermolysis of citric acid and TiO<sub>2</sub> (Scheme 1). The as-synthesized heterostructure shows superior photocatalytic activity for H<sub>2</sub> generation from water in the presence of Pt under visible light irradiation, which can be attributed to extended absorption of visible light due to CQDs as well as improved intimate contact of CQDs with TiO<sub>2</sub>, which facilitates efficient charge separation in CQDs.



Scheme 1. Schematic representation of CQD/Pt/TIO<sub>2</sub> by co-thermolysis of citric acid and TiO<sub>2</sub>.

# 2. Experimental Section

- **2.1 Chemicals and Materials.** TiO<sub>2</sub>(5-10nm, anatase), H<sub>2</sub>PtCI<sub>6</sub>·6H<sub>2</sub>O and citric acid were purchased from Aladdin Industrial Corporation (Shanghai). All other reagents were used as received without further purification.
- **2.2 Synthesis of Pt@TiO2 Composites.** The Pt@TiO2 composites were prepared using photodeposition method (Scheme 1). Typically, 100 mg of TiO2 and 2.7 mg of H<sub>2</sub>PtCI<sub>6</sub>·6H<sub>2</sub>O were dissolved in 16 mL of ascorbic acid solution (AA, 0.1 M in water). The solution was purged with N<sub>2</sub> to remove O<sub>2</sub>. The mixture was then irradiated by 405 nm LED lamp for 24 h under stirring. The resulting Pt preloaded TiO<sub>2</sub> was separated by centrifugation and washed with 10 mL deionized water twice. The theoretical wt% in the Pt preloaded TiO<sub>2</sub> was calculated to be 1%, and the sample was marked as 1%Pt@TiO<sub>2</sub>. To investigate the effect of the Pt content on the photocatalytic H<sub>2</sub> evolution rate, the Pt@TiO<sub>2</sub> composites with different contents of Pt (0, 0.5, 1, 2, and 3wt%) were also prepared and labelled as X%Pt@TiO<sub>2</sub> (X=0, 0.5, 1, 2, and 3). The actual proportion of Pt in each sample was measured using ICP-AES (Table S2).
- 2.3 Synthesis of CQDs/X%@TiO2 Composites. The CQDs/X%Pt@TiO2 composites were obtained by a thermolysis method according to literature report with minor modification (scheme 1).<sup>29</sup> Typically, as-prepared 1%Pt@TiO2 were suspended in 4 ml of deionized water, where 1 g of citric acid was then added to the suspension. The suspension was ultrasonicated for 5 mins and then pyrolyzed in a furnace for 40 h at 180°C under air. The residual dark brown solid was grinded and washed with 4 ml of DMF, 10 ml of deionized water twice, and 10 ml of ethanol successively. The products were then dried under vacuum. CQDs that were not directly deposited onto Pt@TiO2 were removed during these procedures. 95 mg of CQDs/Pt@TiO2 was collected, and these products were labelled as CQDs/1%Pt@TiO2. CQDs/Pt@TiO2 with different Pt contents were synthesized using the same procedure described above and labelled as

CQDs/X%Pt@TiO<sub>2</sub>(X=0, 0.5, 1, 2, and 3). A pure CQDs sample was also synthesized following the same procedure as control sample.

2.4 Standard Characterization. UV-visible absorption spectra of the samples were taken using a Shimadzu U-3900H spectrometer. FTIR spectra were recorded on a Perkin Elmer Frontier spectrophotometer. The XRD patterns were performed using a Rigaku Ultima IV XRD diffractometer with Cu Kα radiation. TEM was taken with a FEI Tecnai-G20 electron microscope with an accelerating voltage of 200 kV. XPS measurements were performed on a Thermo ESCALAB 250 using monochromatic Al K□ radiation (1846.6 eV) as the X-ray source. The steady state and time-resolved fluorescence were measured using QM40 Quanta Master system by Photo Technology International (PTI) equipped with PicoMaster time-correlated single-photon counting (TCSPC). The pulsed excitation was provided by 415 nm LED. The emission was detected at 500 nm. For emission and TCSPC measurement, 0.1 mg sample was dispersed in methanol in 1x1 cm quartz cuvette. The determination of Pt proportion was conducted on a PerkinElmer Optima 8000. The amount of Pt in the hybrids was determined by ICP-AES analysis and the amount of CQDs was determined by weight loss after calcining under air at 550°C for 2 h.

2.5 Photochemical Hydrogen Generation. Photocatalytic reactions were performed in a 13 mL vial under the illumination of 405 nm LED lamp and the output optical power was adjusted to 90 mW. In a general process, a certain amount of CQDs/X%Pt@TiO<sub>2</sub> was suspended in 4 mL of ascorbic acid (0.1 M in H<sub>2</sub>O). The vial was sealed, degassed with N<sub>2</sub>, treated with ultrasound and transferred to photocatalysis apparatus. The amount of evolved hydrogen was quantified by Agilent 490 micro gas chromatograph with a TCD detector (N<sub>2</sub> carrier gas, 5 Å molecular sieve column) by taking 100 μL of the headspace of the vial.

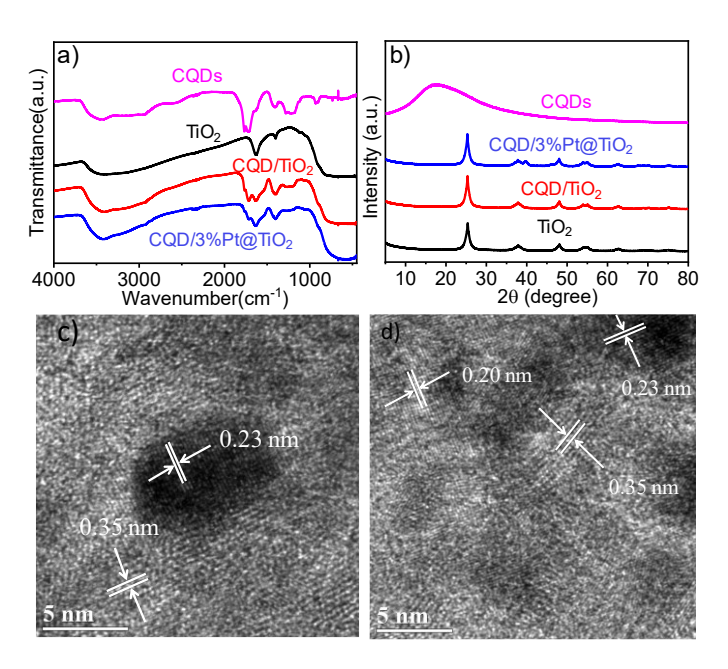


Figure 1. FTIR spectra (a) and XRD patterns (b) of CQDs, TiO<sub>2</sub>, CQDs/TiO<sub>2</sub> and CQDs/3%Pt@TiO<sub>2</sub> nanocomposites. HRTEM images (c) and (d) of CQDs/3%Pt@TiO<sub>2</sub> hybrids.

# 3. Results and Discussion

Figure 1a shows the FTIR spectra of CQDs/3%Pt@TiO<sub>2</sub> nanocomposites. The FTIR spectra of pure TiO<sub>2</sub> and CQDs and CQDs/TiO<sub>2</sub> were also shown for comparison. The characteristic absorption peaks of the Pure CQDs at 1766 cm<sup>-1</sup> and 1717 cm<sup>-1</sup> can be attributed to the stretching vibration of C=O and C=C, respectively. <sup>30-32</sup> The peaks at 3424 cm<sup>-1</sup> and 1405 cm<sup>-1</sup> can be assigned to the stretching vibration of O-H and in-plane bending vibration of C-O-H, respectively, and the peak at 1221 cm<sup>-1</sup> can be attributed to the stretching vibration of C-O. The absence of absorption band corresponding to C-H and =C-H vibration around 3000 cm<sup>-1</sup> indicates that the CQDs were well thermolyzed. <sup>30-32</sup> For pure TiO<sub>2</sub>, the absorption peaks at 3401 cm<sup>-1</sup> and 1626 cm<sup>-1</sup> can be attributed to the stretching and bending vibration of O-H in TiO<sub>2</sub>,

respectively.<sup>22</sup> The broad absorption band below 1000 cm<sup>-1</sup> belongs to TiO<sub>2</sub> characteristic absorption.<sup>21, 33</sup> All of these absorption features are observed in the spectra of CQDs/3%Pt@TiO<sub>2</sub> sample and other CQDs/X%Pt@TiO<sub>2</sub> (Figure S1a), suggesting the presence of both CQDs and TiO<sub>2</sub> in the composites. However, the broad absorption band below 1000 cm<sup>-1</sup> in the spectra of CQDs/3%Pt@TiO<sub>2</sub> composites shows a red shift compared to that of TiO<sub>2</sub>. This is consistent with the literature data and can be attributed to the combination of the Ti–O–Ti and Ti–O–C vibrations.<sup>30</sup>

Figure 1b shows the XRD patterns of CQDs, TiO<sub>2</sub>, CQDs/TiO<sub>2</sub> and CQDs/3%Pt@TiO<sub>2</sub>. The diffraction peaks at 25.4°(101), 37.9°(004), 48.1°(200), 54.0°(105), 55.1°(211) and 62.7°(204) correspond to the characteristic peaks of anatase TiO<sub>2</sub>.<sup>31, 34-35</sup> These peaks are all observed in the XRD patterns of CQDs/X%Pt@TiO<sub>2</sub> samples (Figure 1b and Figure S1b), suggesting that the introduction of CQDs have negligible effect on the crystal structure of TiO<sub>2</sub>. The diffraction peaks at 39.7° and 46.3° can be attributed to the (111) and (200) facets of Pt, respectively, <sup>36-37</sup> suggesting the presence of Pt in CQDs/X%Pt@TiO<sub>2</sub>. For pure CQDs, there is a broad peak at 18.4°, indicating that CQDs exist as amorphous phase.<sup>29, 38</sup> As this peak is absent in all CQDs/X%Pt@TiO<sub>2</sub> samples, we believe that CQDs do not exist in the nanocomposites as pure form, i.e. they are directly connected with TiO<sub>2</sub> as a thin film.<sup>34</sup>

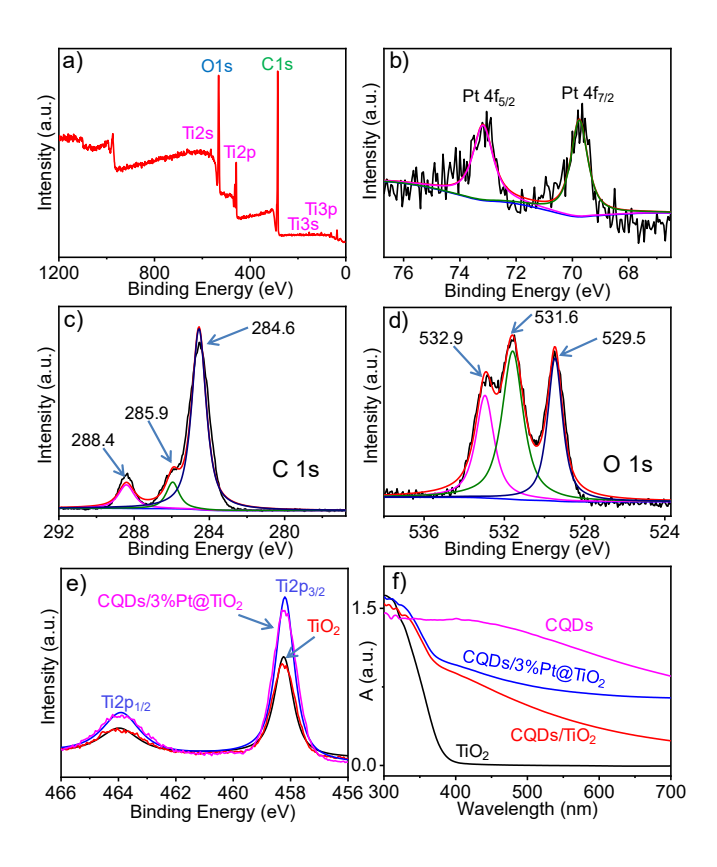


Figure 2. XPS spectra for full survey (a), Pt 4f (b), C 1s (c), O 1s (d), and Ti 2p (e) of CQDs/3%Pt@TiO<sub>2</sub> nanocomposites. (f) UV-visible diffuse reflectance spectra of CQDs, TiO<sub>2</sub>, CQDs/TiO<sub>2</sub>, and CQDs/3%Pt@TiO<sub>2</sub> nanocomposites.

Figure 1c and 1d shows the HRTEM images of CQDs/3%Pt@TiO<sub>2</sub> nanocomposites, where TiO<sub>2</sub> appears to be nanosheets in size of around 200-300 nm (Figure S2a). The image at Figure 1c reveals a spherical morphology about 6-7 nm in diameter with a lattice spacing of around 0.23 nm, which can be assigned to (111) plane of Pt particles.<sup>39-40</sup> The lattice spacing of around 0.35 nm can be attributed to (101) plane of TiO<sub>2</sub>,<sup>30</sup> which matches well with the XRD data (Figure 1b). The lattice spacing of 0.20 nm as shown in Figure 1d can be assigned to (101) plane of CQDs<sup>34</sup>, indicating that CQDs exist as a sheet instead of a spherical particle. These results together confirm the successful coupling of CQDs and Pt@TiO<sub>2</sub>.

Furthermore, the chemical components and surface property of pure TiO<sub>2</sub> and CQDs/3%Pt@TiO<sub>2</sub> nanocomposites were examined using XPS. The full-scale XPS spectrum (Figure 2a) and high-resolution Pt (4f) XPS spectrum (Figure 2b) of CQDs/3%Pt@TiO<sub>2</sub> confirm the existence of Ti, O, C and Pt, respectively. The binding energies of 69.8 (Pt 4f<sub>7/2</sub>) and 73.2 eV (Pt  $4f_{5/2}$ ) are attributed to metallic Pt (Figure 2b), which are slightly lower than literature data, <sup>36</sup>-<sup>37</sup> suggesting that Pt is in a more electron-rich environment. Figure 2c shows the deconvoluted C(1s) XPS spectrum of the CQDs/3%Pt@TiO<sub>2</sub>. The typical peaks at 284.6 eV, 285.9 eV and 288.4 eV are attributed to the C-C (graphite), C-O and O=C-O bonds, 30-32, 34-35 respectively, which further supports the presence of CQDs in CQDs/3%Pt@TiO2 nanocomposites, consistent with the HRTEM and FTIR results. The peaks at 529.5 eV, 531.6 eV and 532.9 eV in the deconvoluted O(1s) XPS spectrum (Figure 2d) are assigned to the Ti-O, C-O and O-H bonds, respectively, which further supports the presence of the CQDs. 30-32, 34 The Ti(2p) XPS spectra of the CQDs/3%Pt@TiO<sub>2</sub> and TiO<sub>2</sub> were also collected (Figure 2e). The peaks at 464.0 and 458.3 eV observed in the CQDs/3%Pt@TiO<sub>2</sub>, corresponding to Ti(2p<sub>1/2</sub>) and Ti(2p<sub>3/2</sub>), respectively, are slightly shifted towards higher binding energy by 0.1 eV compared with those in pure TiO<sub>2</sub>, suggesting that the chemical environment of Ti in the CQDs/3%Pt@TiO<sub>2</sub> has changed due to the interaction between the TiO<sub>2</sub> and CQDs.<sup>30, 34</sup> The contents of Pt, C, O and Ti in CQDs/3%Pt@TiO<sub>2</sub> are calculated to be 0.077%, 62.8%, 30.6% and 6.5%, respectively. The large abundance of C and O suggests that CQDs are mainly located on the surface of the nanocomposites.

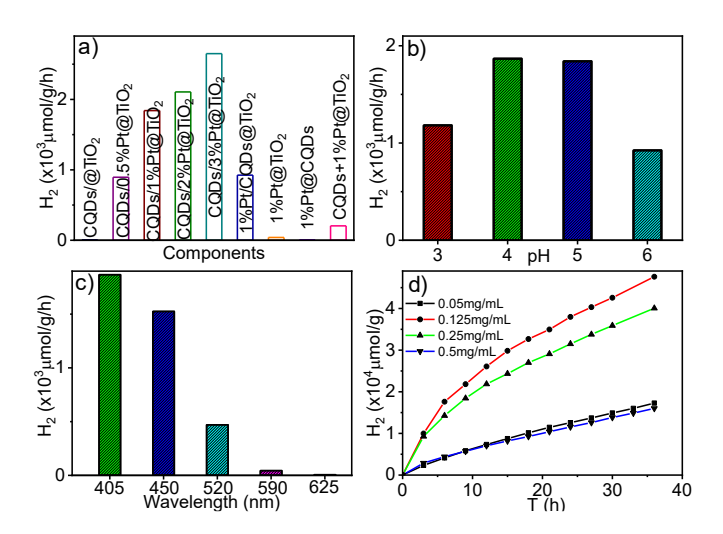


Figure 3. (a) The dependence of H<sub>2</sub> generation efficiency on components (a), pH value (b), and illumination wavelength (c). (d) The H<sub>2</sub> generation time profile CQDs/1%Pt@TiO<sub>2</sub>. The photocatalytic experiments were performed with 405 nm LED illumination except for c where LED lamp with different wavelengths were used.

Figure 2f shows the UV-Visible diffuse reflectance spectra of pure TiO<sub>2</sub>, CQDs, CQDs/TiO<sub>2</sub> and CQDs/3%Pt@TiO<sub>2</sub> nanocomposites. The pure TiO<sub>2</sub> exhibits less intense absorption in the visible region of 400–800 nm due to its wide band gap. However, CQDs/TiO<sub>2</sub> and CQDs/3%Pt@TiO<sub>2</sub> composite samples exhibit absorption increase in the region of 400-700 nm, which can be ascribed to the extended absorption in the visible region due to CQDs. The presence of CQDs and Pt on TiO<sub>2</sub> was further supported by EDS (Figure S3 and Table S1) and element mapping (Figure S4), where we found that C and Pt were homogeneously distributed in the hybrid sample. The actual amount of (Pt, C) for the hybrids (Table S2) are (0, 25.6), (0.28, 24.3), (0.57, 19.2), (1.34, 12.8), and (2.21, 10.2) in percentile for CQDs/TiO<sub>2</sub>, CQDs/0.5%Pt@TiO<sub>2</sub>, CQDs/1%Pt@TiO<sub>2</sub>, CQDs/2%Pt@TiO<sub>2</sub>, CQDs/3%Pt@TiO<sub>2</sub>, respectively.

The photocatalytic activity of these nanocomposites was evaluated under illumination of LED lamp. The catalytic conditions were first optimized to obtain the optimum condition for H<sub>2</sub> production. Figure 3a shows the dependence of H<sub>2</sub> production on catalyst components. It can be seen that Pt is essential for the H<sub>2</sub> production reaction as the sample without the presence of Pt shows significantly lower efficiency (6.2 µmol/g/h H<sub>2</sub>) than the systems with Pt. While Pt preloaded pure TiO<sub>2</sub> (40 µmol/g/h) or CQDs (6.0 µmol/g/h) can also catalyze the hydrogen evolution reaction, the catalytic activity of these systems is much lower than the nanocomposites including all three components, where the catalytic activity was boosted to 895, 1841, 2106, 2650 µmol/g/h for the composites with 0.5%, 1%, 2% and 3% Pt contents, respectively, suggesting that both CQDs and TiO<sub>2</sub> are essential for efficient generation of H<sub>2</sub>. Because the samples with higher loading Pt (2% and 3% Pt) did not increase the catalytic activity proportionally, CQDs/1%Pt@TiO<sub>2</sub> was selected for further optimization of reaction conditions. While H<sub>2</sub> evolution efficiency increases with decreasing proportion of CQDs on the hybrid samples, the dependence of efficiency on increasing Pt proportion is much more prominent. This is likely due to that the amount of CQDs in each sample is sufficient to reduce TiO2 and the presence of larger amount of CQDs may cause more severe light scattering.

Figure 3b Shows the dependence of H<sub>2</sub> production on pH of ascorbic acid (AA), from which we found that the system with pH=4.0 showed catalytic efficiency of 1867 μmol/g/h, which is the best among all systems and was thus selected for further optimization of H<sub>2</sub> evolution. Note that the pH values show negligible change before and after mixing with catalysts (Table S4). Figure 3c shows the dependence of H<sub>2</sub> production on illumination wavelengths. While the H<sub>2</sub> production efficiency decreases with increasing illumination wavelength, which agrees well with the absorption spectrum of CQDs (Figure 2f), the system shows notable catalytic activity under

450 nm (1525 μmol/g/h) and 520 nm (470 μmol/g/h) where TiO<sub>2</sub> has negligible absorption, suggesting that CQDs significantly improved the visible light absorption of the system and lead to ultimate enhanced photocatalytic activity in visible region. In addition, the dependence of H<sub>2</sub> production on the concentrations of CQDs&1%Pt@TiO2 in the catalytic mixture was evaluated (Figure 3d). It was found that the system with 0.125 mg/mL CQDs&1%Pt@TiO<sub>2</sub> produces highest efficiency of H<sub>2</sub> (3323 µmol/g/h) and the system with 0.25mg/mL of CQDs&1%Pt@TiO<sub>2</sub> results into the photon-to-H<sub>2</sub> conversion efficiency (0.57%) in the initial 3h. To the best of our knowledge, this indeed represents the system with highest H<sub>2</sub> generation efficiency among all CQDs sensitized materials, <sup>31, 34-35</sup> largely promising their application in solar-to-fuel conversion. In terms of the stability, the H<sub>2</sub> production does not decrease after 36 hours' illumination, suggesting that the hybrid system is at least stable for 36 hours. Surely, there were some changes appeared to the hybrid according to the FTIR comparing before and after 36 h's irradiation (Figure S5), the characteristic absorption peaks of CQDs at 1766 cm<sup>-1</sup> and 1717 cm<sup>-1</sup> decreased, and became a shoulder of 1626 cm<sup>-1</sup>, which is the bending vibration of O-H in TiO<sub>2</sub>.

It is interesting to note that the sequence for the introduction of Pt to the nanohybrids affects the catalytic activity. As shown in Figure 3a, the catalyst with preloaded Pt prior to the introduction of CQDs exhibited better catalytic activity than those when CQDs were introduced first. This was further confirmed by a control experiment, where we evaluated the H<sub>2</sub> generation efficiency of a system prepared from mechanically mixing 0.25mg/mL of CQDs with 1%Pt@TiO<sub>2</sub>, which shows much lower efficiency, i. e. 205 μmol/g/h, representing 11% of activity for CQDs&1%Pt@TiO<sub>2</sub> system. These results together suggest the importance of thermolysis of CQDs and TiO<sub>2</sub>.

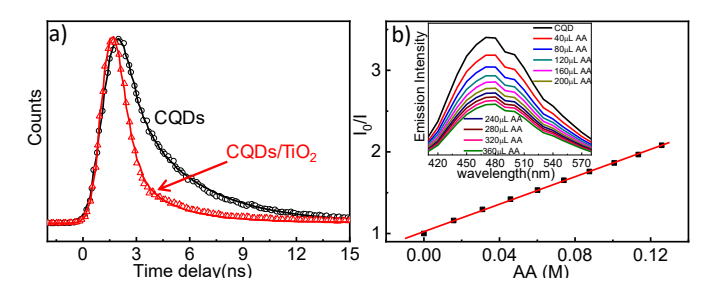


Figure 4. (a) The emission lifetime of CQDs and CQDs@TiO<sub>2</sub>. (b) The Stern-Volmer plot of CQDs, from which the reductive quenching constant is 6.25 x 10<sup>9</sup> M<sup>-1</sup>S<sup>-1</sup>. The inset shows the emission spectra of CQDs in the presence of different concentrations of AA.

The enhanced  $H_2$  production efficiency in this work compared to the previously reported systems<sup>31, 34-35</sup> is likely due to improved interaction between CQDs and TiO<sub>2</sub>, which facilitates charge transfer from CQDs to TiO<sub>2</sub>. Shown in Figure 4a is the emission lifetime decay kinetics measured by time-resolved fluorescence spectroscopy following 415 nm excitation. The significantly decreased emission lifetime of CQDs in the presence of TiO<sub>2</sub> can be attributed to charge transfer process from CQDs to TiO<sub>2</sub>. The emission kinetics for both samples can be fit by a two-exponential decay function (Table S2), from which we found that the emission lifetimes of CQDs and CQDs/TiO<sub>2</sub> were 1.35 ns ( $\tau_{int}$ ) and 0.65 ns ( $\tau_{obs}$ ), respectively (Table S3), which results into a charge transfer time 1.3 ns ( $\tau_{ET}$ ), which is obtained according to  $1/\tau_{obs} = 1/\tau_{ET} + 1/\tau_{int}$ . Because electron transfer time from AA to CQDs was found to be 1.6 ns based on Stern Volmer plot (Figure 4b and SI), which is comparable to charge transfer time from CQDs to TiO<sub>2</sub>, we believe that both reductive and oxidative quenching pathways are responsible for  $H_2$  generation. The mechanism is significantly different from the recent literatures reported results, wherein, CQDs acted as an electrons accepter or transfering bridge.

## 4. Conclusions

In summary, we report a facile synthesis of CQDs sensitized TiO<sub>2</sub>/Pt nanohybrids through onestep thermolysis of CQDs and Pt@TiO<sub>2</sub>, which can efficiently generate H<sub>2</sub> from water with high stability. We found that this method not only simplifies the synthetic procedure for fabricating CQDs sensitized Pt@TiO<sub>2</sub> but also enhances the interaction of CQDs with TiO<sub>2</sub>, which facilitates charge transfer process from CQDs to TiO<sub>2</sub> and eventually enhance H<sub>2</sub> generation efficiency. This work suggests that thermolysis way provide a new approach for developing CQDs based nanocomposites as efficient solar-to-fuel catalytic materials.

#### ASSOCIATED CONTENT

**Supporting Information**. FTIR spectra, XRD patterns, TEM images, diffuse reflectance UV-visible absorption spectra of CQDs, TiO<sub>2</sub>, and CQDs/X%Pt@TiO<sub>2</sub>; Raman spectra, Pt and CQDs proportion, fitting parameters for TCSPC.

#### **AUTHOR INFORMATION**

# **Corresponding Author**

\*Jier Huang (jier.huang@marquette.edu)

\*Yulu Zhou (zhouyl@upc.edu.cn)

## **Author Contributions**

The manuscript was written through contributions of all authors. All authors have given approval to the final version of the manuscript.

#### ACKNOWLEDGMENT

This work was supported by National Science Foundation of China (201801250). S.Y., J.R., and J.H. acknowledge the support from National Science Foundation (DMR-1654140).

## REFERENCES

- 1. Gratzel, M., Artificial Photosynthesis Water Cleavage into Hydrogen and Oxygen by Visible-Light. *Accounts Chem. Res.* **1981**, *14*, 376-384.
- 2. Chen, X. B.; Shen, S. H.; Guo, L. J.; Mao, S. S., Semiconductor-based Photocatalytic Hydrogen Generation. *Chem. Rev.* **2010**, *110*, 6503-6570.
- 3. Lehn, J. M.; Sauvage, J. P., Chemical Storage of Light Energy Catalytic Generation of Hydrogen by Visible-Light or Sunlight Irradiation of Neutral Aqueous-Solutions. *Nouv. J. Chim.* **1977**, *1*, 449-451.
- 4. Yang, H. G.; Liu, G.; Qiao, S. Z.; Sun, C. H.; Jin, Y. G.; Smith, S. C.; Zou, J.; Cheng, H. M.; Lu, G. Q., Solvothermal Synthesis and Photoreactivity of Anatase TiO<sub>2</sub> Nanosheets with Dominant {001} Facets. *J. Am. Chem. Soc.* **2009**, *131*, 4078-4083.
- 5. Pan, J.; Liu, G.; Lu, G. M.; Cheng, H. M., On the True Photoreactivity Order of {001}, {010}, and {101} Facets of Anatase TiO<sub>2</sub> Crystals. *Angew. Chem., Int. Ed.* **2011**, *50* (9), 2133-2137.
- 6. Mazierski, P.; Nadolna, J.; Nowaczyk, G.; Lisowski, W.; Winiarski, M. J.; Klimczuk, T.; Kobylanski, M. P.; Jurga, S.; Zaleska-Medynska, A., Highly Visible-Light-Photoactive Heterojunction Based on TiO<sub>2</sub> Nanotubes Decorated by Pt Nanoparticles and Bi<sub>2</sub>S<sub>3</sub> Quantum Dots. *J. Phys. Chem. C* **2017**, *121*, 17215-17225.
- 7. Wang, F. L.; Wong, R. J.; Ho, J. H.; Jiang, Y. J.; Amal, R., Sensitization of Pt/TiO<sub>2</sub> Using Plasmonic Au Nanoparticles for Hydrogen Evolution under Visible-Light Irradiation. *Acs Appl. Mater. Inter.* **2017**, *9*, 30575-30582.
- 8. Gratzel, M., Solar Energy Conversion by Dye-Sensitized Photovoltaic Cells. *Inorg. Chem.* **2005**, *44*, 6841-6851.
- 9. Zheng, Q.; Kang, H.; Yun, J.; Lee, J.; Park, J. H.; Baik, S., Hierarchical Construction of Self-Standing Anodized Titania Nanotube Arrays and Nanoparticles for Efficient and Cost-Effective Front-Illuminated Dye-Sensitized Solar Cells. *Acs Nano* **2011**, *5*, 5088-5093.
- 10. Asahi, R.; Morikawa, T.; Ohwaki, T.; Aoki, K.; Taga, Y., Visible-Light Photocatalysis in Nitrogen-Doped Titanium Oxides. *Science* **2001**, *293*, 269-271.
- 11. Burda, C.; Lou, Y. B.; Chen, X. B.; Samia, A. C. S.; Stout, J.; Gole, J. L., Enhanced Nitrogen Doping in TiO<sub>2</sub> Nanoparticles. *Nano Lett.* **2003**, *3*, 1049-1051.

- 12. Momeni, M. M.; Ghayeb, Y., Fabrication, Characterization and Photoelectrochemical Behavior of Fe-TiO<sub>2</sub> Nanotubes Composite Photoanodes for Solar Water Splitting. *J. Electroanal. Chem.* **2015**, *751*, 43-48.
- 13. Long, L. Z.; Li, J.; Wu, L. P.; Li, X. J., Enhanced Photocatalytic Performance of Platinized CdS/TiO<sub>2</sub> by Optimizing Calcination Temperature of TiO<sub>2</sub> Nanotubes. *Mat. Sci. Semicon. Proc.* **2014**, *26*, 107-111.
- 14. Wang, C. J.; Kwon, K. W.; Odlyzko, M. L.; Lee, B. H.; Shim, M., PbSe Nanocrystal/TiOx Heterostructured Films: A Simple Route to Nanoscale Heterointerfaces and Photocatalysis. *J. Phys. Chem. C* **2007**, *111*, 11734-11741.
- 15. Li, H. T.; He, X. D.; Kang, Z. H.; Huang, H.; Liu, Y.; Liu, J. L.; Lian, S. Y.; Tsang, C. H. A.; Yang, X. B.; Lee, S. T., Water-Soluble Fluorescent Carbon Quantum Dots and Photocatalyst Design. *Angew. Chem., Int. Ed.* **2010**, *49*, 4430-4434.
- 16. Zhang, H. C.; Huang, H.; Ming, H.; Li, H. T.; Zhang, L. L.; Liu, Y.; Kang, Z. H., Carbon Quantum Dots/Ag<sub>3</sub>PO<sub>4</sub> Complex Photocatalysts with Enhanced Photocatalytic Activity and Stability under Visible Light. *J. Mater. Chem.* **2012**, *22*, 10501-10506.
- 17. Han, Y. Z.; Huang, H.; Zhang, H. C.; Liu, Y.; Han, X.; Liu, R. H.; Li, H. T.; Kang, Z. H., Carbon Quantum Dots with Photoenhanced Hydrogen-Bond Catalytic Activity in Aldol Condensations. *ACS Catal.* **2014**, *4*, 781-787.
- 18. Tian, J.; Leng, Y. H.; Zhao, Z. H.; Xia, Y.; Sang, Y. H.; Hao, P.; Zhan, J.; Li, M. C.; Liu, H., Carbon Quantum Dots/Hydrogenated TiO<sub>2</sub> Nanobelt Heterostructures and Their Broad Spectrum Photocatalytic Properties under UV, Visible, and Near-Infrared Irradiation. *Nano Energy* **2015**, *11*, 419-427.
- 19. Zhang, J.; Zhang, X. Y.; Dong, S. S.; Zhou, X.; Dong, S. S., N-Doped Carbon Quantum Dots/TiO<sub>2</sub> Hybrid Composites with Enhanced Visible Light Driven Photocatalytic Activity toward Dye Wastewater Degradation and Mechanism Insight. *J. Photoch. Photobio. A* **2016**, *325*, 104-110.
- 20. Ren, P.; Fu, X. B.; Zhang, Y. M., Carbon Quantum Dots-TiO<sub>2</sub> Nanocomposites with Enhanced Catalytic Activities for Selective Liquid Phase Oxidation of Alcohols. *Catal. Lett.* **2017**, *147*, 1679-1685.
- 21. Yu, H. J.; Zhao, Y. F.; Zhou, C.; Shang, L.; Peng, Y.; Cao, Y. H.; Wu, L. Z.; Tung, C. H.; Zhang, T. R., Carbon Quantum Dots/TiO<sub>2</sub> Composites for Efficient Photocatalytic Hydrogen Evolution. *J. Mater. Chem. A* **2014**, *2*, 3344-3351.
- 22. Pan, J. Q.; Sheng, Y. Z.; Zhang, J. X.; Wei, J. M.; Huang, P.; Zhang, X.; Feng, B. X., Preparation of carbon quantum dots/TiO<sub>2</sub> nanotubes composites and their visible light catalytic applications. *J. Mater. Chem. A* **2014**, *2*, 18082-18086.
- 23. Li, H.; Shi, W. N.; Huang, W. C.; Yao, E. P.; Han, J. B.; Chen, Z. F.; Liu, S. S.; Shen, Y.; Wang, M. K.; Yang, Y., Carbon Quantum Dots/TiOx Electron Transport Layer Boosts

- Efficiency of Planar Heterojunction Perovskite Solar Cells to 19%. *Nano Lett.* **2017**, *17*, 2328-2335.
- 24. Zhuo, S. J.; Shao, M. W.; Lee, S. T., Upconversion and Downconversion Fluorescent Graphene Quantum Dots: Ultrasonic Preparation and Photocatalysis. *Acs Nano* **2012**, *6*, 1059-1064.
- 25. Ming, H.; Ma, Z.; Liu, Y.; Pan, K. M.; Yu, H.; Wang, F.; Kang, Z. H., Large Scale Electrochemical Synthesis of High Quality Carbon Nanodots and Their Photocatalytic Property. *Dalton T.* **2012**, *41*, 9526-9531.
- 26. Wang, J.; Gao, M. M.; Ho, G. W., Bidentate-Complex-Derived TiO<sub>2</sub>/Carbon Dot Photocatalysts: In Situ Synthesis, Versatile Heterostructures, and Enhanced H<sub>2</sub> Evolution. *J. Mater. Chem. A* **2014**, *2*, 5703-5709.
- 27. Liu, J. C.; Zhu, W. Y.; Yu, S. Y.; Yan, X. L., Three Dimensional Carbogenic Dots/TiO<sub>2</sub> Nanoheterojunctions with Enhanced Visible Light-Driven Photocatalytic Activity. *Carbon* **2014**, *79*, 369-379.
- 28. Zhang, Z.-M.; Zhang, T.; Wang, C.; Lin, Z.; Long, L.-S.; Lin, W., Photosensitizing Metal–Organic Framework Enabling Visible-Light-Driven Proton Reduction by a Wells–Dawson-Type Polyoxometalate. *J. Am. Chem. Soc.* **2015**, *137*, 3197-3200.
- 29. Martindale, B. C.; Hutton, G. A.; Caputo, C. A.; Reisner, E., Solar Hydrogen Production Using Carbon Quantum Dots and a Molecular Nickel Catalyst. *J. Am. Chem. Soc.* **2015**, *137*, 6018-6025.
- 30. Yu, H.; Zhao, Y.; Zhou, C.; Shang, L.; Peng, Y.; Cao, Y.; Wu, L.-Z.; Tung, C.-H.; Zhang, T., Carbon Quantum Dots/TiO<sub>2</sub> Composites for Efficient Photocatalytic Hydrogen Evolution. *J. Mater. Chem. A* **2014**, *2*, 3344-3351.
- 31. Pan, J.; Sheng, Y.; Zhang, J.; Wei, J.; Huang, P.; Zhang, X.; Feng, B., Preparation of Carbon Quantum Dots/ TiO<sub>2</sub> Nanotubes Composites and Their Visible Light Catalytic Applications. *J. Mater. Chem. A* **2014**, *2*, 18082-18086.
- 32. Qin, J.; Zeng, H., Photocatalysts Fabricated by Depositing Plasmonic Ag Nanoparticles on Carbon Quantum Dots/Graphitic Carbon Nitride for Broad Spectrum Photocatalytic Hydrogen Generation. *Appl. Catal. B: Environ.* **2017**, *209*, 161-173.
- 33. Zhang, H.; Lv, X. J.; Li, Y. M.; Wang, Y.; Li, J. H., P25-Graphene Composite as a High Performance Photocatalyst. *Acs Nano* **2010**, *4*, 380-386.
- 34. Tang, Y.; Hao, R.; Fu, Y.; Jiang, Y.; Zhang, X.; Pan, Q.; Jiang, B., Carbon Quantum Dot/Mixed Crystal TiO<sub>2</sub> Composites via a Hydrogenation Process: An Efficient Photocatalyst for the Hydrogen Evolution Reaction. *RSC Advances* **2016**, *6*, 96803-96808.
- 35. Xiang, Q.; Yu, J.; Jaroniec, M., Enhanced Photocatalytic H<sub>2</sub>-Production Activity of Graphene-Modified Titania Nanosheets. *Nanoscale* **2011**, *3*, 3670-3678.

- 36. Liang, Y.; Zhang, H.; Zhong, H.; Zhu, X.; Tian, Z.; Xu, D.; Yi, B., Preparation and Characterization of Carbon-Supported PtRuIr Catalyst with Excellent CO-Tolerant Performance for Proton-Exchange Membrane Fuel Cells. *J. Catal.* **2006**, *238*, 468-476.
- 37. Nie, R.; Wang, J.; Wang, L.; Qin, Y.; Chen, P.; Hou, Z., Platinum Supported on Reduced Graphene Oxide as a Catalyst for Hydrogenation of Nitroarenes. *Carbon* **2012**, *50*, 586-596.
- 38. Ming, H.; Ma, Z.; Liu, Y.; Pan, K.; Yu, H.; Wang, F.; Kang, Z., Large Scale Electrochemical Synthesis of High Quality Carbon Nanodots and Their Photocatalytic Property. *Dalton transactions* **2012**, *41*, 9526-9531.
- 39. Jiang, L.; Sun, G.; Sun, S.; Liu, J.; Tang, S.; Li, H.; Zhou, B.; Xin, Q., Structure and Chemical Composition of Supported Pt–Sn Electrocatalysts for Ethanol Oxidation. *Electrochimica Acta* **2005**, *50*, 5384-5389.
- 40. Li, Q.; Zong, L.; Li, C.; Yang, J., Photocatalytic Reduction of CO<sub>2</sub> on MgO/TiO<sub>2</sub> Nanotube Films. *Applied Surface Science* **2014**, *314*, 458-463.
- 41. Gao, Y.; Hou, F.; Hu, S.; Wu, B.; Wang, Y. Zhang, H.; Jiang, B.; Fu, H., Graphene Quantum Dots Modified Hexagonal Tubular Carbon Nitride for Visible-light Photocatalytic Hydrogen Evolution. *ChemCatChem* **2018**, *10*, 1330-1335.
- 42. Ding, Y.; Gao, Y.; Li, Z., Carbon Quantum Dots (CQDs) and Co(dmgH)<sub>2</sub>PyCl Synergistically Promote Photocatalytic Hydrogen Evolution over Hexagonal ZnIn<sub>2</sub>S<sub>4</sub>. *Applied Surface Science* **2018**, *462*, 255-262.

## TOC

